



Climate impact on the development of Pre-Classic Maya civilization

Kees Nooren, Wim Z Hoek, Brian J Dermody, Didier Galop, Sarah Metcalfe,
Gerald Islebe, Hans Middelkoop

► To cite this version:

Kees Nooren, Wim Z Hoek, Brian J Dermody, Didier Galop, Sarah Metcalfe, et al.. Climate impact on the development of Pre-Classic Maya civilization. *Climate of the Past Discussions [Climate of the Past Preprints]*, 2018, 14 (8), pp.1253-1273. <10.5194/cp-2018-15>. <hal-01860353>

HAL Id: hal-01860353

<https://univ-tlse2.hal.science/hal-01860353v1>

Submitted on 23 Aug 2018

HAL is a multi-disciplinary open access archive for the deposit and dissemination of scientific research documents, whether they are published or not. The documents may come from teaching and research institutions in France or abroad, or from public or private research centers.

L'archive ouverte pluridisciplinaire **HAL**, est destinée au dépôt et à la diffusion de documents scientifiques de niveau recherche, publiés ou non, émanant des établissements d'enseignement et de recherche français ou étrangers, des laboratoires publics ou privés.



HAL Authorization



Climate impact on the development of Pre-Classic Maya civilization

Authors

Kees Nooren¹, Wim Z. Hoek¹, Brian J. Dermody¹, Didier Galop², Sarah Metcalfe³, Gerald Islebe⁴ and Hans Middelkoop¹.

Affiliations

¹Utrecht University, Faculty of Geosciences, 3508 TC Utrecht, The Netherlands;

²Université Jean Jaurès, CNRS, UMR 5602 GEODE, 31058 Toulouse, France;

³University of Nottingham, School of Geography, Nottingham NG7 2RD, UK

⁴El Colegio de la Frontera Sur, Unidad Chetumal Herbario, Chetumal, AP 424 Quintana Roo, Mexico;

Correspondence to: Kees Nooren (k.nooren@gmail.com)

Keywords

Pre-Classic Maya period, Central Maya Lowlands, climate record, beach ridges, palaeo-precipitation, 500-yr periodicity, 2.8 ka event.

Abstract

The impact of climate change on the development and disintegration of Maya civilization has long been debated. The lack of agreement among existing palaeoclimatic records from the region has prevented a detailed understanding of regional-scale climatic variability, its climatic forcing mechanisms, and its impact on the ancient Maya. We present two new palaeo-precipitation records for the Central Maya Lowlands, spanning the Pre-Classic period (1800 BCE – 250 CE), a key epoch in the development of Maya civilization. Lake Tuspan's diatom record is indicative of precipitation changes at a local scale, while a beach ridge elevation record from world's largest late Holocene beach ridge plain provides a regional picture. We identify centennial-scale variability in palaeo-precipitation that significantly correlates with the North Atlantic $\delta^{14}\text{C}$ atmospheric record, with a comparable periodicity of approximately 500 years, indicating an important role of North Atlantic atmospheric-oceanic forcing on precipitation in the Central Maya Lowlands. The Early Pre-Classic period was characterized by relatively dry conditions, shifting to wetter conditions during the Middle Pre-Classic period, around the well-known 850 BCE (2.8 ka) event. We propose that this wet period may have been unfavorable for agricultural intensification in the Central Maya Lowlands, explaining the relatively delayed development of Maya civilization in this area. A return to relatively drier conditions during the Late Pre-Classic period coincides with rapid agricultural intensification in the region and the establishment of major cities.

1. Introduction

During the last decades, a wealth of new data has been gathered to understand human-environmental interaction and the role of climate change in the development and disintegration of societies in the Maya Lowlands (e.g., Akers et al., 2016; Douglas et al., 2015, 2016; Dunning et al., 2012, 2015; Lentz et al., 2014; Turner and Sabloff, 2012). Previous studies have emphasized the impact of prolonged droughts and their possible link with social downturn, such as the Pre-Classic Abandonment and the Classic Maya Collapse (Ebert et al., 2017; Hoggarth et al., 2016; Lentz et al., 2014; Kennett et al., 2012; Medina-Elizalde et al., 2010, 2016; Hodel et al., 1995, 2001, 2005; Haug et al., 2003). Less attention has been given to episodes of excessive rain and floods that may also have severely impacted ancient Maya societies (e.g. Iannone et al., 2014). This may be testified by the fact that floods, as well as droughts, are an important theme depicted in the remaining ancient Maya codices (Fig. 1) (Thompson, 1972), and Mayan mythological stories (Valásquez García, 2006).

One of the main challenges in palaeoclimatic reconstructions is to unravel climate from human induced changes. Maya societies played a key role in the formation of the landscape, but the degree of human induced impact remains highly debated (Hansen, 2017; Beach et al., 2015; Ford and Nigh, 2015). For example, it is proposed that the increase in sedimentation rate after 1000 BCE at Lake Salpeten (Anselmetti et al., 2007) and Peten-Itza (Mueller et al., 2009) is related to human induced soil erosion. However, other high resolution lake records from the area do not show a significant increase in sedimentation rate during the Pre-Classic or Classic period (e.g. Wahl et al., 2014), and past volcanic activity could have been responsible for the deposition of 'Maya Clay' (Nooren et al., 2017a). Palynological records from the Central Maya Lowlands (CML, Fig. 2) show no evidence of widespread land clearance and agriculture before ~400 BCE (Wahl et al., 2007; Islebe et al., 1996; Leyden et al.,



1987), and there is growing consensus that the decline in the percentage of lowland tropical forest pollen during the Pre-Classic period (Galop et al., 2004; ; Islebe et al., 1996; Leyden et al., 1987) was caused by climatic drying instead of deforestation (Torrescano and Islebe, 2015; Wahl et al., 2014; Mueller et al., 2009).

In this paper, we present two new palaeo-precipitation records reflecting precipitation changes in the CML. The records span the Pre-Classic period (1800 BCE – 250 CE), when Maya societies in the CML transformed from predominantly mobile hunter-gatherers in the Early Pre-Classic Period (e.g. Inomata et al., 2015; Coe, 2011; Lohse, 2010), to complex sedentary societies that founded impressive cities like El Mirador by the later part of the Pre-Classic period (Hansen, 2017; Inomata and Henderson, 2016). The period of rapid growth in these centralized societies likely occurred much later than previously thought, likely sometime after the start of the Late Pre-Classic period around 400 BCE (Inomata and Henderson, 2016). This raises the question for the reason behind the delayed development of societies in this area, which was to become the core area of Maya civilization during the following Classic period (250 – 900 CE). We hypothesize that climate during the Middle Pre-Classic Period (1000 – 400 BCE) may have been less stable than recently reported (Ebert et al., 2017), and could have been unfavorable for intensification of maize-based agriculture, which formed the underlying subsistence economy responsible for the development of many neighbouring Mesoamerican societies during this period.

The CML have been intensively studied, and several well-dated speleothem, palynological, and limnological records have been obtained for this area (Díaz et al., 2017; Akers et al., 2016; Douglas et al., 2015; Wahl et al., 2014; Kennett et al., 2012; Mueller et al., 2009; Metcalfe et al., 2009; Domínguez-Vázquez and Islebe, 2008; Galop et al., 2004; Rosenmeier et al., 2002; Islebe et al., 1996) (Fig. 2 and A1). However, palaeo-precipitation signals from these records and those from adjacent areas in the Yucatan and Central Mexico exhibit large differences among records (Fig. A2), making the reconstruction and interpretation of larger-scale precipitation for the region a challenge (Lachniet et al., 2013, 2017; Douglas et al., 2016; Metcalfe et al., 2015). Existing climate reconstructions mostly represent local changes and are predominantly based on oxygen isotope variability, although some new proxies have been introduced recently (e.g. Díaz et al., 2017; Douglas et al., 2015).

We present a regional-scale palaeo-precipitation record for the CML, extracted from world's largest late Holocene beach ridge sequence at the Gulf of Mexico coast (Fig. 2B). The beach ridge record captures changes in river discharge resulting from precipitation patterns over the entire catchment of the Usumacinta River and thus represents regional changes in precipitation over the CML (Nooren et al., 2017b). Currently the annual discharge of the Usumacinta river is approximately 2000 m³/s, corresponding to ~40 % of the excess or effective rain falling in the 70,700 km² large catchment (Nooren et al., 2017b). Mean annual precipitation within the catchment is ~2150 mm, with 80 % falling during the boreal summer, related to the North American or Mesoamerican Monsoon system (Lachniet et al., 2013, 2017; Metcalfe et al., 2015). The interpretation of the beach ridge record is supported by a new multi-proxy record from Lake Tuspan, an oligosaline lake situated within the CML, receiving most of its water from a relatively small catchment of 770 km² (Fig. 2).

Regional palaeo-precipitation signal

The coastal beach ridges consist of sandy material originating from the Grijalva and Usumacinta rivers, topped by wind-blown beach sand (Nooren et al., 2017b). Although multiple factors determine the final elevation of the beach ridges, it has been shown that during the period 1775 ± 95 BCE to 30 ± 95 CE (at 1σ), roughly coinciding with the Pre-Classic period, beach ridge elevation has primarily been determined by the discharge of the Usumacinta river, in a counter-intuitive manner: low elevation anomalies of the beach ridges occur in periods with increased river sediment discharge, which in turn is the product of high precipitation within the river catchment. Under these conditions, beach ridges develop relatively rapidly, and are exposed to wind for a shorter period. In contrast, during periods of drought, sediment supply to the coast is reduced, resulting in a decreased seaward progradation rate of the beach ridge plain. This leaves a longer period for aeolian accretion on the beach ridges near the former shoreline, resulting in higher beach ridges (Nooren et al., 2017b). Hence, variations in beach ridge elevation reflect changes in rainfall over the Usumacinta catchment, and thereby represent catchment-aggregated precipitation, instead of a local signal. The very high progradation rates and the very robust age-distance model (Fig. A3), with uncertainties of the calibrated ages not exceeding 60–70 years (at 1σ), effectively allow the reconstruction of palaeo-precipitation at centennial time scale.



Local palaeo-precipitation signal: Lake Tuspan record

Diatom communities within oligo- to hypersaline lakes are strongly influenced by lake water salinity (Reed, 1998; Gasse et al., 1995), and we therefore determined diatom assemblage changes within the Lake Tuspan sediment record (Fig. 3) to reconstruct palaeo-salinities of the lake water, reflecting palaeo-precipitation in the lake's catchment. During dry periods, a reduced riverine input of fresh water and a lowering of the lake level enhance the effect of evaporation and increase the salinity of the lake water. The first principal component (PC-1) of the variability in the diatom assemblages is interpreted as an indicator of lake water salinity (Fig. 3). This interpretation is supported by the fact that high PC-1 values are accompanied by relatively high percentages of *Plagiotropis arizonica* (Fig. A4), a diatom species characteristic of high-conductivity water bodies (Czarnecki and Blinn, 1978).

2. Methods

Lake Tuspan

Two parallel cores, Tuspán core B and C, were taken with a Russian corer (type GYK) in shallow water near the inflow of the Rio Dulce, not far from core A which has been studied for pollen (Galop et al., 2004). Semi-quantitative analyses of Si, S, K, Ca, Ti, Mn and Fe were conducted on both cores with an X-ray fluorescence core scanner (type AVAATECH) at 0.5 cm intervals. Deposits of large floods were identified on the basis of elevated concentrations of Si, Fe, Ti and Al, with peak concentrations exceeding at least the one standard deviation threshold above the mean.

Core C was investigated for amorphous silica, charred plant fragments, and diatoms (Fig. 3, and A5). The core was subsampled at 4-12 cm contiguous intervals, each interval representing 25-80 years. In addition, 37 1-cm samples (representing ~6.5 yr) were processed using the method outlined by Battarbee (1973) to determine diatom concentrations and to determine short time variability (decadal scale). Subsamples were treated with HCl (10 %) to remove calcium carbonate. Large organic particles were removed by wet sieving (250 µm mesh), and charred plant fragments > 250 µm were counted under a dissection microscope. Remaining organic material was removed by heavy liquid separation using a sodiumpolywolframate solution with a density of 2.0 g/cm³. A silicious residue, denoted 'amorphous silica' was subsequently removed by heavy liquid separation using a sodiumpolywolframate solution with a density of 2.3 g/cm³, and dry weight was determined after drying of the samples at 105°C. Slides were prepared from the remaining material. Diatoms were identified, counted and reported as percentages of the total diatom sum, excluding the small and often dominant *Denticula elegans* and *Nitzschia amphibia* species. These species show a large variability on short time scales (Fig. A6), and are not indicative for changes at centennial time scale. We relate changes in diatom assemblages mainly to lake water salinity changes. The first principal component on the entire assemblage (PC-1) is interpreted as a palaeosalinity indicator. Diatom taxonomy is mainly after Patrick and Reimer (1966; 1975) and Novelo, Tavera, and Ibarra (2007). We identified *Plagiotropis arizonica* following Czarnecki and Blinn (1978), and *Mastogloia calcarea* following Lee et al. (2014).

The age-depth model for core C is based on seven AMS radiocarbon dated terrestrial samples and stratigraphical correlation with core A (Fleury et al., 2014). We used a linear regression between the available radiocarbon dated samples (Fig. A7) which is comparable with the age-depth model by Fleury et al. (2014) for the time window between ~2500 BCE and 1000 CE.

Beach ridge sequence

Beach ridges elevations were extracted from a Digital Elevation Model (DEM) of the coastal plain along the transects indicated in Fig. 2 (Nooren et al., 2017b). The DEM is based on LiDAR data originally acquired in April-May 2008 and processed by Mexico's National Institute of Statistics and Geography (INEGI), Mexico. The relative beach ridge elevation is defined as the difference between the beach ridge elevation and the long-term (~500 yr) running mean (Fig. A3).

Wavelet transfer functions

The relation between our beach ridge and diatom record and other palaeo-precipitation records from the Maya Lowlands and nearby regions (figure A1 and A2) were investigated by wavelet coherence (CWT) analyses using the software developed by Grinsted et al. (2004). The record of drift ice from the North Atlantic (Bond et al., 2001) is bimodally distributed, oscillating between periods of low and high concentrations of hematite stained grains. The timeseries was therefore transformed into a record of



percentiles based on its cumulative distribution function to avoid leakage of the square wave into frequency bands outside the fundamental period (Grinsted et al., 2004).

3. Climate change in the CML during the Pre-Classic period

Early Pre-Classic Period (1800 – 1000 BCE)

The Lake Tuspan diatom record (Fig. 3) indicates relatively dry conditions, comparable to those during the preceding Late Archaic Period (~5000 – 1800 BCE). Despite the predominantly dry conditions, large floods still occurred, as demonstrated by the repetitive input of fluvial material into the lake. These flood events are identifiable as distinctive dark layers of detrital sediment within the calcareous lake deposits, and are characterized by elevated concentrations of amorphous silica and charred plant fragments (Fig. 3 and A4). The average recurrence time of large floods was approximately 50 years, and periods with highest fluvial sediment input in Lake Tuspan coincided with periods of increased input of charcoal into Lake Peten-Itza (Schüpbach et al., 2015) (Fig. A2). Because the CML were still sparsely populated during the Early Pre-Classic period (Inomata et al., 2015) we relate the presence of charcoal to the occurrence of wildfires.

The beach ridge record indicates a drying trend that culminated in a prolonged dry period at the end of the Early Pre-Classic period. Although this exceptionally dry phase is less apparent from Lake Tuspan's diatom record (Fig. 3), it has been recorded at many other sites within the CML. At Lake Puerto Arturo, high $\delta^{18}\text{O}$ values on the gastropod *Pyrgophorus* sp. indicate that this was the driest period since 6300 BCE (Wahl et al., 2014), and the recently extended and improved speleothem $\delta^{18}\text{O}$ record from Macal Chasm indicates that this dry period was probably at least as severe as any prolonged droughts during the Classic and Post-Classic Period (Akers et al., 2016). Dry conditions are reflected in high $\text{Ca}/\Sigma(\text{Ti,Fe,Al})$ values at Lake Peten-Itza (Mueller et al., 2009), indicating elevated authigenic carbonate (CaCO_3) precipitation relative to the input of fluvial detrital elements (Ti, Fe and Al) during this period, and water level at this large lake must have dropped by at least 7 m (Mueller et al., 2009).

Middle Pre-Classic Period (1000 – 400 BCE)

Both the beach ridge and the Lake Tuspan diatom records indicate a change to wetter conditions around 1000-850 BCE, causing major changes in hydrological conditions in the CML (Fig. 3). The diatom assemblages in the Lake Tuspan record show a major change in composition. Species indicative of meso- to polysaline water almost completely disappear, and are replaced by species indicating fresh water conditions (Fig. 3 (PC1) and A4). In the lake sediments, this transition is also marked by a lithological shift from laminated to more homogeneous sediments that lack repetitive flood layers, while charred plant fragments are almost absent until ~400 BCE. Similar abrupt lithological transitions were reported from Lake Chichancanab (Hodell et al., 1995) and Lake Peten-Itza (Mueller et al., 2009), and Wahl et al. (2014) describe a regime shift at Puerto Arturo. The sudden reduction in charred plant fragments around ~1000 BCE at Lake Tuspan coincides with reduced concentrations of charcoal at Lake Peten-Itza (Fig. A2) (Schubach et al., 2015) and Laguna Tortuguero, Puerto Rico (Burney and Pigott Burney, 1994) indicating rapid climatic changes over a large spatial scale.

Late Pre-Classic period (400 BCE – 250 CE)

The diatom record at Lake Tuspan (Fig. 3) shows a general increase in lake water salinity, indicating a gradual shift to drier conditions in the Late Pre-Classic Period. The beach ridge record (Fig. 3) indicates that a relatively dry period occurred by the onset of the Late Pre-Classic period, which has not been identified in other proxy records from the region (Fig. A2), although high *Pinus* pollen percentages in the pollen record from Petapilla pond near Copan (McNeil, 2010) during this period may indicate dry conditions, as high *Pinus* pollen percentage at highland sites could be indicative for drier conditions (Domínguez-Vázquez and Islebe, 2008).

Precipitation variability over long time scales

The observed general drying trend over the last thousands of years may be related to the southward shift of the ITCZ during the late Holocene. The shift occurred in response to orbitally-forced changes in insolation (Haug et al., 2001), causing a gradual Northern Hemisphere cooling versus Southern Hemisphere warming (Fig. 3), thereby shifting the ITCZ towards the warming southern hemisphere (Schneider et al., 2014). A more northerly position of the ITCZ during the Pre-Classic period may be related to stronger easterly tradewinds and the less frequent occurrence of cold fronts during the Pre-Classic period, as beach ridge morphological changes suggest (Nooren et al., 2017b).



Centennial scale precipitation variability

Wavelet coherence (WTC) analysis (Grinsted et al., 2004) indicates in-phase coherence between the beach ridge record and the recently extended and revised calcite $\delta^{18}\text{O}$ speleothem record from Macal-Chasm cave (Akers et al., 2016) (Fig. A8). The in-phase relationship between the two records is significant above a 5% confidence level at centennial timescales during the Pre-Classic Period. We did not find significant relationships between the beach ridge record and other palaeo-precipitation records from the CML, nor with records from the Yucatan and Central Mexico (Fig. A2), except for a significant in-phase coherence at centennial time scale with the *Pyrgophorus* sp. $\delta^{18}\text{O}$ record from Lake Chichancanab (Hodell et al., 1995).

The coherence between the beach ridge record and the well-dated Macal-Chasm speleothem record give us confidence that these records reflect regionally coherent variability at centennial timescales during the Pre-Classic period. Interestingly, the beach ridge record is significantly in anti-phase with the North Atlantic ice drift record (Bond et al., 2001) and the Northern Hemispheric atmospheric $\delta^{14}\text{C}$ record during the Pre-Classic Period (Reimer et al., 2013) (Fig. 4), suggesting an important role of North Atlantic atmospheric-oceanic forcing on precipitation in the CML. The Northern Hemispheric atmospheric $\delta^{14}\text{C}$ record shows a 512-yr periodicity (Stuiver and Braziunas, 1993), which is similar to the observed ~500 year periodicity of the beach ridge record during the Pre-Classic period. Such a centennial scale periodicity is not apparent in Lake Tuspan's diatom record (Fig. 3), nor in any of the other palaeo-precipitation records from the Maya Lowlands (Fig. A2), but has been identified in the Ti record from Lake Juanacatlán in the highlands of Central Mexico (Jones et al., 2015). This periodicity has been related to the intensity of the North Atlantic thermohaline circulation and variations in solar activity (Stuiver and Braziunas, 1993).

The coherence with fluctuations in solar irradiance is most evident during the 2.8 ka event, related to the Homeric Grand Solar Minimum. At this time, a strong decrease in the total solar irradiance resulted in higher atmospheric ^{14}C production and a change to cooler and wetter condition in the Northern Hemisphere (e.g. Van Geel et al., 1996), and apparently also a shift to wetter conditions in the CML, evident from our two new palaeo-precipitation records (Fig. 3). This correlation should not be used as an analogue for modern precipitation variability, when periods of lower solar activity are associated with lower Usumacinta River discharge and hence less precipitation in the CML (Fig. A9).

A similar precipitation response to the late Holocene southward shift of the ITCZ for both Northern South America and the Maya Lowlands has previously been suggested (Haug et al., 2003), implying that the beach ridge record should be in-phase with the Cariaco Ti record (Haug et al., 2001). Although the Cariaco record indicates large centennial scale variability in precipitation over Northern South America (Fig. 3), this variability is not significantly correlated with the beach-ridge record. The correlation slightly improved using an updated age-depth model for the Cariaco record (Fig. A10), but remains insignificant, probably due to uncertainties in the chronological control of both records or due to a more prominent influence of the Northern Atlantic climatic forcing mechanisms in the Maya Lowlands.

4. Precipitation versus human development in the CML

Our records indicate that the Early Pre-Classic period in the CML was relatively dry. During this period, the CML were still sparsely populated by moving hunter-gatherers. It is highly likely that before maize became sufficiently productive to sustain sedentism, the karstic lowlands were less attractive for humans than the coastal wetlands along the Gulf of Mexico and Pacific coast, where natural resources were abundantly present to successfully sustain a hunting/gathering subsistence system (Inomata et al., 2015). Reliance on cultivated crops, most notably maize, rapidly increased after the onset of the Middle Pre-Classic period around 1000 BCE (Rosenswig et al., 2015). Between 1000 – 850 BCE, under still dry conditions, there is evidence for increased maize agriculture in the Pacific flood basin (Rosenswig et al., 2015), and within the Olmec area at the Gulf of Mexico coast (Arnold III, 2009), and maize grains (AMS ^{14}C dated to 875 ± 29 BCE) have been found as far as Ceibal within the CML (Inomata et al., 2015). We speculate that wetter conditions after 850 BCE might have been unfavorable for a further development of intensive agriculture in the CML. This is supported by palynological evidence, indicating that widespread land clearance and agriculture activity did not occur before ~400 BCE (Wahl et al., 2007; Galop et al., 2004; Islebe et al., 1996; Leyden et al., 1987), despite some early local agricultural activity (Wahl et al., 2014; Rushton et al., 2013; McNeil et al., 2010; Galop et al., 2004). A return to drier conditions during the Late Pre-Classic period coincided



with an expansion of maize-based agriculture in the CML, and communities within the Maya Lowlands show a strong and steady development with relatively uniform ceramic and architectural styles (Hansen, 2017; Inomata and Henderson, 2016). Hence, major development of Maya civilization in the Central Maya Lowlands occurred only after the onset of the Late Pre-Classic period, when climate became progressively drier, in line with earlier findings that drier conditions were favorable for agricultural development in the CML (Wahl et al., 2014).

Acknowledgements

This research is supported by the Netherlands Organization for Scientific Research (NWO-grant 821.01.007). The LiDAR data was generously provided by INEGI, Mexico. We acknowledge Philippe Martinez, Jacques Giraudeau and Pierre Carbonel for the XRF core scan measurements, and we would like to thank Peter Douglas, Pete Akers and Gerald Haug for providing their data. We thank Konrad Huguen for valuable suggestions to update the age-depth model for Cariaco's sediment core 1002D.

References

- Akers, P.D., Brook, G.A., Railsback, L.B., Liang, F., Iannone, G., Webster, J.W., Reeder, P.P., Cheng, H., and Edwards, R.L., An extended and higher-resolution record of climate and land use from stalagmite MC01 from Macal Chasm, Belize, revealing connections between major dry events, overall climate variability, and Maya sociopolitical changes. *Palaeogr Palaeoclimatol Palaeoecol* 459: 268-288, 2016.
- Amador, J.A., Alfaro, E.J., Lizano, O.G., and Magaña, V.O., Atmospheric forcing of the eastern tropical Pacific: A review. *Progress in Oceanography* 69: 101-142, 2006.
- Anselmetti, F.S., Hodell, D.A., Ariztegui, D., Brenner, M., and Rosenmeier, M.F., Quantification of soil erosion rates related to ancient Maya deforestation. *Geology* 35: 915-918, 2007.
- Arnold III, P.J., Settlement and subsistence among the Early Formative Gulf Olmec. *J Anthropol Archaeol* 28: 397-411, 2009.
- Banco Nacional de Datos de Aguas Superficiales, Conagua.
<http://www.conagua.gob.mx/CONAGUA07/Contenido/Documentos/Portada BANDAS.htm>
[conagua.gob.mx/Bandas/Bases_Datos_Presas/](http://www.conagua.gob.mx/Bandas/Bases_Datos_Presas/), consulted January 2017.
- Bhattacharya, T., Byrne, R., Böhm, H., Wogau, K., Kienel, U., Ingram, B.L., and Zimmerman, S., Cultural implications of late Holocene climate change in the Cuenca Oriental, Mexico. *Proc Natl Acad Sci USA* 112(6), 1693-1698, 2015.
- Batterbee, R.W., A new method for estimating absolute microfossil numbers with special reference to diatoms. *Limnol Oceanogr* 18: 647-653, 1973.
- Beach, T., Luzzadder-Beach, S., Cook, D., Dunning, N., Kennett, D.J., Krause, S., Terry, R., Trein, D., and Valdez, F., Ancient Maya impacts on the Earth's surface: An Early Anthropocene analog? *Quat Sci Rev* 124: 1-30, 2015.
- Bernal, J.P., Lachniet, M., McCulloch, M., Mortimer, G., Morales, P., and Cienfuegos, E., A speleothem record of Holocene climate variability from southwestern Mexico. *Quat Res* 75:104-113, 2011.
- Bond, G., Kromer, B., Beer, J., Muscheler, R., Evans, M.N., Showers, W., Hoffmann, S., Lotti-Bond, R., Hajdas, I., and Bonani, G., Persistent Solar Influence on North Atlantic Climate During the Holocene. *Science* 294: 2130-2136, 2001.
- Bronk Ramsey, C., Oxcal 4.2.; <http://c14.arch.ox.ac.uk/oxcal.html>, 2016.
- Bronk Ramsey, C., Bayesian analysis of radiocarbon dates. *Radiocarbon* 51: 337-360, 2009.



- 359 Burney, D.A., and Pigott Burney, L., Holocene Charcoal Stratigraphy from Laguna Tortuguero, Puerto
360 Rico, and the Timing of Human Arrival on the Island. *J Archaeol Sci* 21: 273-281, 1994.
361
- 362 Coe, M.D., *The Maya*, eight edition, Thames and Hudson, London, UK, 2011.
363
- 364 Curtis, J.H., and Hodell, D.A., Climate Variability on the Yucatan Peninsula (Mexico) during the Past
365 3500 Years, and Implications for Maya Cultural Evolution. *Quat Res* 46: 37-47, 1996.
366
- 367 Curtis, J.H., Brenner, M., Hodell, D.A., Balser, R.A., Islebe, G.A., and Hooghiemstra, H., A
368 multiproxy study of Holocene environmental change in the Maya Lowlands of Peten, Guatemala. *J*
369 *Paleolimnol* 19: 139-159, 1998.
370
- 371 Czarnecki, D.B., and Blinn, D.W., Observations on Southwestern Diatoms. I. *Plagiotropis arizonica* N.
372 Sp. (Bacillariophyta, Entomoneidaceae), a large Mesohalobous Diatom. *Trans Am Microsc Soc* 97:
373 393-396, 1978.
374
- 375 Díaz, K.A., Pérez, L., Correa-Metrio, A., Franco-Gaviria, J.F., Echeverria, P., Curtis, J., and Brenner,
376 M., Holocene environmental history of tropical, mid-altitude Lake Ocotlito, México, inferred from
377 ostracodes and non-biological indicators. *Holocene* 27, 1308-1317, 2017.
378
- 379 Domínguez-Vázquez, G., and Islebe, G.A., Protracted drought during the late Holocene in the
380 Lacandon rain forest, Mexico. *Veg Hist Archaeobot* 17: 327-333, 2008.
381
- 382 Douglas, P.M.J., Demarest, A.A., Brenner, M., and Canuto, M.A., Impacts of Climate Change on the
383 Collapse of Lowland Maya Civilization. *Annu Rev Earth Planet Sci* 44: 613-645, 2016.
384
- 385 Douglas, P.M.J., Pagani, M., Canuto, M.A., Brenner, M., Hodell, D.A., Eglinton, T.I., and Curtis, J.H.,
386 Drought, agricultural adaptation, and sociopolitical collapse in the Maya Lowlands. *Proc Natl Acad Sci*
387 *USA* 112: 5607-5612, 2015.
388
- 389 Dunning, N.P., Beach, T.P., and Luzzadder-Beach, S., Kax and kol: Collapse and resilience in lowland
390 Maya civilization. *Proc Natl Acad Sci USA* 109(10): 3652-3657, 2012.
391
- 392 Dunning, N.P., McCane, C., Swinney, T., Purtill, M., Sparks, J., Mann, A., McCool, J.-P., and Ivenso,
393 C., Geoaarchaeological Investigations in Mesoamerica Move into the 21st Century: A Review.
394 *Geoarchaeology* 30: 167-199, 2015.
395
- 396 Ebert, C.E., Peniche May, N., Culleton, B.J., Awe, J.J., and Kennett, D.J., Regional response to
397 drought during the formation and decline of PreClassic Maya societies. *Quat Sci Rev* 173, 211-235,
398 2017.
399
- 400 Fleury, S., Malaizé, B., Giraudeau, J., Galop, D., Bout-Roumazelles, V., Martinez, P., Charlier, K.,
401 Carbonel, P., and Arnaud, M.-C., Impacts of Mayan land use on Laguna Tuspan watershed (Petén,
402 Guatemala) as seen through clay and ostracode analysis. *J Archaeol Sci* 49: 372-382, 2014.
403
- 404 Ford, A., and Nigh, R., *The Maya Forest Garden: Eight Millennia of Sustainable Cultivation of the*
405 *Tropical Woodland*, Taylor and Francis, London, New York, 2015.
406
- 407 Galop, D., Lemonnier, E., Carozza, J.M., and Metailie, J.P., Bosques, milpas, casas y aguadas de
408 antaño. In: *La Joyanca, ciudad maya del noroeste del Peten (Guatemala)*, Arnaud C. et Breuil-
409 Martinez V. (eds.). CEMCA, CIRMA, Asociacion Tikal, Guatemala, 55-71, 2004.
410
- 411 Gasse, F., Juggins, S., and Ben Khelifa, L., Diatom-based transfer functions for inferring past
412 hydrochemical characteristics of African lakes. *Palaeogeogr Palaeoclimatol Palaeoecol* 117: 31-54,
413 1995.
414
- 415 Grinsted, A., Moore, J.C., and Jevrejeva, S., Application of the cross wavelet transform and wavelet
416 coherence to geophysical time series. *Nonlinear Processes Geophys* 11: 561-566, 2004.
417



- 418 Hansen, R.D., The Feast Before Famine and Fighting: The Origins and Consequences of Social
419 Complexity in the Mirador Basin, Guatemala. Feast, Famine or Fighting? Multiple Pathways to Social
420 Complexity, Chacon, R.J., and Mendoza, R.G. (eds), Springer, Dordrecht, the Netherlands, pp 305-335,
421 2017.
- 422
- 423 Haug, G.H., Hughen, K.A., Sigman, D.M., Peterson, L.C., and Röhl, U., Southward Migration of the
424 Intertropical Convergence Zone Through the Holocene. *Science* 293, 1304–1308, 2001.
- 425
- 426 Haug, G.H., Gunther, D., Peterson, L.C., Sigman, D.M., Hughen, K.A., and Aeschlimann, B., Climate
427 and the Collapse of Maya Civilization. *Science* 299: 1731-1735, 2003.
- 428
- 429 Hijmans, R.J., Cameron, S.E., Parra, J.L., Jones, P.G., and Jarvis, A., Very high resolution interpolated
430 climate surfaces for global land areas. *Int J of Clim* 25: 1965-1978, 2005.
- 431
- 432 Hodell, D.A., Brenner, M., and Curtis, J.H., Climate and cultural history of the Northeastern Yucatan
433 Peninsula, Quintana Roo, Mexico. *Climatic Change* 83: 215–240, 2007.
- 434
- 435 Hodell D.A., Brenner, M., and Curtis, J.H., Terminal Classic drought in the northern Maya lowlands
436 inferred from multiple sediment cores in Lake Chichancanab (Mexico). *Quat Sci Rev* 24: 1413–1427,
437 2005.
- 438
- 439 Hodell, D.A., Brenner, M., Curtis, J.H., and Guilderson, T., Solar forcing of drought frequency in the
440 Maya lowlands. *Science* 292: 1367–1369, 2001.
- 441
- 442 Hodell, D.A., Curtis, J.H., and Brenner, M., Possible role of climate in the collapse of Classic Maya
443 civilization. *Nature* 375: 391–394, 1995.
- 444
- 445 Hoggarth, J.A., Breitenbach, S.F.M., Culleton, B.J., Ebert, C.E., Mason, M.A., and Kennett, D.J., The
446 political collapse of Chichén Itzá in climatic and cultural context. *Glob Planet Change* 138: 25-42,
447 2016.
- 448
- 449 Iannone, G., The Great Maya Droughts in Cultural Context: Case Studies in Resilience and
450 Vulnerability, Univ Press of Colorado, Boulder, CO, USA, 2014.
- 451
- 452 Inomata, T., and Henderson, L., Time tested: re-thinking chronology and sculptural traditions in
453 Preclassic southern Mesoamerica. *Antiquity* 90: 456-471, 2016.
- 454
- 455 Inomata, T., MacLellan, J., Triadan, D., Munson, J., Burham, M., Aoyama, K., Nasu, H., Pinzón, F.,
456 and Yonenobu, H., Development of sedentary communities in the Maya lowlands: Coexisting mobile
457 groups and public ceremonies at Ceibal, Guatemala. *Proc Natl Acad Sci USA* 112: 4268–4273, 2015.
- 458
- 459 Islebe, G.A., Hooghiemstra, H., Brenner, M., Curtis, J.H., and Hodell, D.A., A Holocene vegetation
460 history from lowland Guatemala. *Holocene* 6: 265–271, 1996.
- 461
- 462 Jones, M.D., Metcalfe, S.E., Davies, S.J., and Noren, A., Late Holocene climate reorganisation and the
463 North American Monsoon. *Quat Sci Rev* 124: 290-295, 2015.
- 464
- 465 Kalnay E., Kanamitsu, M., Kistler, R., Collins, W., Deaven, D., Gandin, L., Iredell, M., Saha, S.,
466 White, G., Woollen, J., Zhu, Y., Chelliah, M., Ebisuzaki, W., Higgins, W., Janowiak, J., Mo, K.C.,
467 Ropelewski, C., Wang, J., Leetmaa, A., Reynolds, R., Jenne, R., and Joseph, D., The NCEP/NCAR
468 Reanalysis 40-year Project. *Bull Am Meteorol Soc* 77: 437–471, 1996.
- 469
- 470 Kennett, D.J., Breitenbach, S.F.M., Aquino, V.V., Asmerom, Y., Awe, J., Baldini, J.U.L., Bartlein, P.,
471 Culleton, B.J., Ebert, C., Jazwa, C., Macri, M.J., Marwan, N., Polyak, V., Prufer, K.M., Ridley, H.E.,
472 Sodemann, H., Winterhalder, B., and Haug, G.H., Development and disintegration of Maya political
473 systems in response to climate change. *Science* 338: 788–791, 2012.
- 474
- 475 Kopp, G., and Lean, J.L., A new, lower value of total solar irradiance: Evidence and climate
476 significance. *Geophys Res Lett* 38: L01706, 2011.
- 477



- 478 Krivova, N.A., Balmaceda, L., and Solanki, S.K., Reconstruction of solar total irradiance since 1700
479 from the surface magnetic flux. *Astron Astrophys* 467: 335–346, 2007.
- 480
- 481 Lachniet, M.S., Asmerom, Y., Bernal, J.P., Polyak, V., and Vazquez-Selem, L., Orbital pacing and
482 ocean circulation-induced collapses of the Mesoamerican monsoon over the past 22,000 y. *Proc Natl*
483 *Acad Sci USA* 110: 9255–9260, 2013.
- 484
- 485 Lachniet, M.S., Asmerom, Y., Polyak, V., and Bernal, J.P., Two millennia of Mesoamerican monsoon
486 variability driven by Pacific and Atlantic synergistic forcing. *Quat Sci Rev* 155: 100–113, 2017.
- 487
- 488 Lee, S., Gaiser, E., VanDeVijver, B., Edlund, M.B., and Spaulding, S.A., Morphology and typification
489 of *Mastogloia smithii* and *M. lacustris*, with descriptions of two new species from the Florida
490 Everglades and the Caribbean region. *Diatom research* 29: 325–350, 2014.
- 491
- 492 Lentz, D.L., Dunning, N.P., Scarborough, V.L., Magee, K.S., Thompson, K.M., Weaver, E., Carr, C.,
493 Terry, R.E., Islebe, G., Tankersley, K.B., Grazioso Sierra, L., Jones, J.G., Buttles, P., Valdez, F., and
494 Ramos Hernandez, C.E., Forests, fields, and the edge of sustainability at the ancient Maya city of Tikal.
495 *Proc Natl Acad Sci USA* 111: 18513–18518, 2014.
- 496
- 497 Leyden, B.W., Man and Climate in the Maya Lowlands. *Quat Res* 28: 407–414, 1987.
- 498
- 499 Lohse, J., Archaic Origins of the Lowland Maya. *Latin American Antiquity* 21: 312–352, 2010.
- 500
- 501 McNeil, C.L., Burney, D.A., and Burney, L.P., Evidence disputing deforestation as the cause for the
502 collapse of the ancient Maya polity of Copan, Honduras. *Proc Natl Acad Sci USA* 107: 1017–1022,
503 2010.
- 504
- 505 Medina-Elizalde, M., Burns, S.J., Polanco-Martinez, J.M., Beach, T., Lases-Hernandez, F., Shen, C.C.,
506 and Wang, H.C., High-resolution speleothem record of precipitation from the Yucatan Peninsula
507 spanning the Maya Preclassic Period. *Glob Planet Change* 138: 93–102, 2016.
- 508
- 509 Medina-Elizalde, M., Burns, S.J., Lea, D.W., Asmerom, Y., von Gunten, L., Polyak, V., Vuille, M.,
510 and Karmalkar, A., High resolution stalagmite climate record from the Yucatan Peninsula spanning the
511 Maya terminal classic period. *Earth Planet Sci Lett* 298: 255–262, 2010.
- 512
- 513 Metcalfe, S.E., Barron, J.A., and Davies, S.J., The Holocene history of the North American Monsoon:
514 ‘known knowns’ and ‘known unknowns’ in understanding its spatial and temporal complexity. *Quat*
515 *Sci Rev* 120: 1–27, 2015.
- 516
- 517 Metcalfe, S., Breen, A., Murray, M., Furley, P., Fallick, A., and McKenzie, A., Environmental change
518 in northern Belize since the latest Pleistocene. *J Quat Sci* 24: 627–641, 2009.
- 519
- 520 Mueller, A.D., Islebe, G.A., Hillesheim, M.B., Grzesik, D.A., Anselmetti, F.S., Ariztegui, D., Brenner,
521 M., Curtis, J.H., Hodell, D.A., and Venz, K.A., Climate drying and associated forest decline in the
522 lowlands of northern Guatemala during the Holocene. *Quat Res* 71: 133–141, 2009.
- 523
- 524 Nooren, K., Hoek, W.Z., Van der Plicht, H., Sigl, M., Van Bergen, M.J., Galop, D., Torrecano-Valle,
525 N., Islebe, G., Huizinga, A., Winkels, T., and Middelkoop, H., Explosive eruption of El Chichón
526 volcano (Mexico) disrupted 6th century Maya civilization and contributed to global cooling. *Geology*
527 45: 175–178, 2017a.
- 528
- 529 Nooren, K., Hoek, W.Z., Winkels, T., Huizinga, A., Van der Plicht, H., Van Dam, R.L., Van Heteren,
530 S., Van Bergen, M.J., Prins, M.A., Reimann, T., Wallinga, J., Cohen, K.M., Minderhoud, P., and
531 Middelkoop, H., The Usumacinta-Grijalva beach-ridge plain in southern Mexico: a high-resolution
532 archive of river discharge and precipitation. *Earth Surf Dynam* 5: 529–556, 2017b.
- 533
- 534 Novelo, E., Tavera, R., and Ibarra, C., Bacillariophyceae from karstic wetlands in Mexico, J. Cramer,
535 Berlin, Germany, 2007.
- 536



- 537 Patrick, R., and Reimer, C.W., *Diatoms of the United States, Vol. I, Monograph 13*, Acad Nat Sci,
538 Philadelphia, USA, 1966.
- 539
- 540 Patrick, R., Reimer, C.W., *Diatoms of the United States, Vol. II, Part I, Monograph 13*, Acad Nat Sci,
541 Philadelphia, USA, 1975.
- 542
- 543 Pollock, A.L., Van Beynen, P.E., De Long, K.L., Polyak, V., Asmerom, Y., and Reeder, P.P., A mid-
544 Holocene paleoprecipitation record from Belize. *Palaeogeogr Palaeoclimatol Palaeoecol* 463: 103-111,
545 2016.
- 546
- 547 Reed, J.M., A diatom-conductivity transfer function for Spanish salt lakes. *J Paleolimnol* 19: 399-416,
548 1998.
- 549
- 550 Reimer, P.J., Bard, E., Bayliss, A., Warren Beck, J., Blackwell, P.G., Ramsey, C.B., Buck, C.E.,
551 Cheng, H., Lawrence Edwards, R., Friedrich, M., Grootes, P.M., Guilderson, T.P., Hafflidason, H.,
552 Hajdas, I., Hatté, C., Heaton, T.J., Hoffmann, D.L., Hogg, A.G., Hughen, K.A., Felix Kaiser, K.,
553 Kromer, B., Manning, S.W., Niu, M., Reimer, R.W., Richards, D.A., Marian Scott, E., Southon, J.R.,
554 Staff, R.A., Turney, C.S.M., and Van der Plicht, J., *IntCal13 and Marine13 radiocarbon age calibration*
555 *curves 0–50,000 years cal BP. Radiocarbon* 55: 1869–1887, 2013.
- 556
- 557 Rosenmeier, M.F., Hodell, D.A., Brenner, M., Curtis, J.H., and Guilderson, T.P., A 4000-year
558 lacustrine record of environmental change in the southern Maya lowlands, Peten, Guatemala. *Quat Res*
559 57: 183–190, 2002.
- 560
- 561 Rosenswig, R.M., VanDerWarker, A.M., Culleton, B.J., and Kennett, D.J., Is it agriculture yet?
562 Intensified maize-use at 1000 cal BC. in the Soconusco and Mesoamerica. *J Antropol Archaeol* 40: 89-
563 108, 2015.
- 564
- 565 Rushton, E.A.C., Metcalfe, S.E., and Whitney, B.S.W., A late-Holocene vegetation history from the
566 Maya Lowlands, Lamanai, Northern Belize. *Holocene* 23: 485-493, 2013.
- 567
- 568 Schneider, T., Bischoff, T., and Haug, G.H., Migrations and dynamics of the intertropical convergence
569 zone. *Nature* 513: 45-53, 2014.
- 570
- 571 Schüpbach, S., Kirchgeorg, T., Colombaroli, D., Beffa, G., Radaelli, M., Kehrwald, N.M., and
572 Barbante, C., Combining charcoal sediment and molecular markers to infer a Holocene fire history in
573 the Maya Lowlands of Petén, Guatemala. *Quat Sci Rev* 115: 123-131, 2015.
- 574
- 575 Steinhilber, F., Abreu, J.A., Beer, J., Brunner, I., Christl, M., Fischer, H., Heikkilä, U., Kubik, P.W.,
576 Mann, M., McCracken, K.G., Miller, H., Miyahara, H., Oerter, H., and Wilhelms, F., 9,400 years of
577 cosmic radiation and solar activity from ice cores and tree rings. *Proc Natl Acad Sci USA* 109: 5967–
578 5971, 2012.
- 579
- 580 Stuiver, M., and Braziunas, T.F., Sun, ocean, climate and atmospheric $^{14}\text{CO}_2$: an evaluation of causal
581 and spectral relationships. *Holocene* 3: 289-305, 1993.
- 582
- 583 Thompson, J.E.S., *A Commentary on the Dresden Codex*, Am Philosophical Society, Philadelphia,
584 USA, 1972.
- 585
- 586 Torrecano-Valle, N., and Islebe, G.A., Holocene paleoecology, climate history and human influence
587 in the southwestern Yucatan Peninsula. *Rev Palaeobot Palynol* 217: 1-8, 2015.
- 588
- 589 Turner II, B.L., and Sabloff, J.A., Classic Period collapse of the Central Maya Lowlands: Insights
590 about human-environment relationships for sustainability. *Proc Natl Acad Sci USA* 109: 13908–13914,
591 2012.
- 592
- 593 USGS, Shuttle Radar Topography Mission (SRTM) 1 Arc-Second Global dataset.
594 <https://ita.cr.usgs.gov/SRTM1Arc>, 2009.
- 595



Valásquez Garcíá, E., The Maya Flood Myth and the Decapitation of the Cosmic Caiman. The PARI Journal 7: 1-10, 2006.

Van Geel, B., Buurman, J., and Waterbolk, H.T., Archaeological and palaeoecological indications for an abrupt climate change in The Netherlands and evidence for climatological teleconnections around 2650 BP. J Quat Sci 11: 451–460, 1996.

Velez, M.I., Curtis, J.H., Brenner, M., Escobar, J., Leyden, B.W., and Popenoe de Hatch, M., Environmental and Cultural Changes in Highland Guatemala Inferred from Lake Amatitlán Sediments. Geomorphology 26: 1-19, 2011.

Wahl, D., Byrne, R., and Anderson, L., An 8700 year paleoclimate reconstruction from the southern Maya lowlands. Quat Sci Rev 103: 19–25, 2014.

Wahl, D., Byrne, R., Schreiner, T., and Hansen, R., Palaeolimnological evidence of late-Holocene settlement and abandonment in the Mirador Basin, Peten, Guatemala. Holocene 17: 813-820, 2007.

Figure captions

Figure 1: The image on page 74 of the Codex Dresden depicts a torrential downpour probably associated with a destructive flood (Thompson, 1972).

Figure 2: A large part of the Central Maya Lowlands (outlined with a red dashed line) is drained by the Usumacinta (Us.) River (A). During the Pre-Classic period this river was the main supplier of sand contributing to the formation of the extensive beach ridge plain at the Gulf of Mexico coast (B). Periods of low rainfall result in low river discharges and are associated with relatively elevated beach ridges. The extend of the watersheds of the Usumacinta and Dulce River is calculated from SRTM 1-arc data (USGS, 2009). Indicated are archaeological sites (squares) and proxy records discussed in the text; Tu= Lake Tuspan, Ch = Lake Chichancanab, PI = Lake Peten-Itza, MC = Macal Chasm Cave, and PA = Lago Puerto Arturo.

Figure 3: Comparison of the Lake Tuspan and beach ridge record (A) with local and proximal records from Macal-Chasm cave (Akers et al., 2016) and the Cariaco basin (Haug et al., 2001)(B). The Cariaco record is conform updated age-depth model (Fig. A10). Climate records related to North Atlantic atmospheric-oceanic forcing are indicated in panel C, including the drift ice reconstruction from the North Atlantic (Bond et al., 2001), the Northern Hemispheric residual atmospheric $\delta^{14}\text{C}$ content (Reimer et al., 2013), the Northern-to Southern hemispheric temperature anomaly (Schneider et al., 2014) and reconstructed Total Solar Irradiance (TSI) (Steinhilber et al., 2012).

Figure 4: Wavelet Transform Coherence (WTC) analysis between the beach ridge record and the Northern Hemispheric atmospheric $\delta^{14}\text{C}$ record (Reimer et al., 2013)(A) and the North Atlantic ice drift record (Bond et al., 2001)(B). The beach ridge record is significantly in anti-phase with both records at approximately 500 yr time scale, indicating an important role of North Atlantic atmospheric-oceanic forcing on precipitation in the Maya Lowlands during the Pre-Classic period. The 5% significance level against red noise is shown as a thick contour. Arrows indicate phase difference, with in-phase relationship between records if arrows point to the right.

Appendix: Additional figures

Figure A1: Location of proxy records indicated in figure A2 and/or mentioned in the main text. A: Northern Maya Lowlands (Tz=Tzabnah, PL=Punta Laguna, RS=Rio Secreto, Ch=Chichancanab and Si=Silvituc), the Central and Southern Maya Lowlands (PA=Puerto Arturo, NRL=New River Lagoon, Tu=Tuspan, PI/Sa=Peten-Itza and Salpeten, MC/CH=Macal Chasm and Chen Ha, and YB=Yok Balum), the Maya Highlands (Oc/Na= Ocotlito and Naja, Am=Amatitlan, and Pet=Petapilla). B: Central Mexico (Jua=Juanacatlan, CdD=Cueva de Diablo, Jx=Juxtlahuacan, and Alj=Aljojuca) and the marine record from the Cariaco (C) basin. Annual precipitation (1950-2000) calculated with WorldClim version 1.4 (release3); Hijmans et al. (2005). Long term (1958-1998) mean ITCZ position and wind at 925 hPa (m.s^{-1}) for July after Amador et al. (2006), based on NCED/NCAR Reanalysis data (Kalnay et al., 1996).



Figure A2a: Palaeoprecipitation records from the Central Maya Lowlands and Yucatan; Beach ridge elevation and Tuspan diatom record (this study), compiled record of Central Peten and Yucatan (Douglas et al., 2016), Salpeten and Chichancanab dD wax-corr. (Douglas et al., 2015), Salpeten $\delta^{18}\text{O}$ (Rosenmeier et al., 2012), Peten-Itza $\delta^{18}\text{O}$ (Curtis et al., 1998), Puerto Arturo $\delta^{18}\text{O}$ (Wahl et al., 2014), Macal Chasm $\delta^{18}\text{O}$ (Akers et al., 2016), Chen Ha $\delta^{18}\text{O}$ (Pollock et al., 2016), Yok Balum $\delta^{18}\text{O}$ (Kennett et al., 2012), Rio Secreto $\delta^{18}\text{O}$ (Medina-Elizalde et al., 2016), Silvituc DV-pollen (Torrescano-Valle and Islebe, 2015), Chichancanab S and $\delta^{18}\text{O}$ (Hodell et al., 1995), Punta Laguna $\delta^{18}\text{O}$ (Hodell et al., 2007), and Tzabnah $\delta^{18}\text{O}$ (Medina-Elizalde et al., 2010).

Figure A2b: Proxy records from the Central Maya Lowlands, the Maya Highlands and Central Mexico. Peten-Itza charcoal (Schüpbach et al., 2015), Peten-Itza pollen (Islebe et al., 1996), Amatitlan Aulacoseira and Pinus (Velez et al., 2011), Petapilla Pinus (McNeil et al., 2010), Naja Pinus (Domínguez-Vázquez and Islebe, 2008), Ocotalito Sr (Díaz et al., 2017), Aljojuca $\delta^{18}\text{O}$ (Bhattacharya et al., 2015), Cueva del Diablo $\delta^{18}\text{O}$ (Bernal et al., 2011), Juxtlahuaca $\delta^{18}\text{O}$ (Lachniet et al., 2015, 2017), and Juanacatlan Ti -15 point running mean (Jones et al., 2015).

Figure A3: Age-distance model for beach ridge transect B (after Nooren et al., 2017b).

Figure A4: Summarized proxy record of Lake Tuspan sediment core C. The 1-4 cm thick dark palaeoflood-layers contrast with the predominantly light coloured calcareous deposits, and are characterized by elevated detrital input, resulting in elevated concentrations of Si (cps = counts per second), amorphous silica (% of dry weight), and charred plant fragments (number of particles/g dw). Only the relative abundance of 'key' diatom species are shown here and the small and often dominant *Denticula elegans* and *Nitzschia amphibia* species were excluded from the diatom sum. The first Principal Component axis (PC-1) is interpreted as a lake water salinity indicator, with low values corresponding to high salinity waters, reflecting relatively dry conditions. Notice abrupt change around 1000 BCE.

Figure A5: Diatom record for lake Tuspan core C. Diatom concentration (*1000 valves/g dw) were determined on 37 selected 1-cm samples and diatom percentages (only the 'key species' are shown here) were determined on the 123 subsamples at 4-12 cm contiguous intervals. The small and often dominant *Denticula elegans* and *Nitzschia amphibia* species were excluded from the diatom sum.

Figure A6: Detailed diatom record around one of the larger flood event ~1200 BCE

Figure A7: Age-depth model for Tuspan core C. The age-depth model is based on a linear interpolation between calibrated ages of radiocarbon dated terrestrial macroremains from core A (Galop et al., 2004) and core C (Fleury et al., 2014). The model is most reliable for ages between ~2500 BCE and 1000 CE.

Figure A8: Wavelet Transform Coherence (WTC) analysis between the beach ridge record and the Macal Chasm $\delta^{18}\text{O}$ record (Akers et al., 2016). The 5% significance level against red noise is shown as a thick contour. Arrows indicate phase difference, with in-phase relationship between records if arrows point to the right.

Figure A9: Mean annual discharge of the Usumacinta river at Boca del Cerro (Banco Nacional de Datos de Aguas Superficiales, consulted in January 2017) compared with the total solar irradiance (TSI). The TSI is comprised of the reconstruction from 1700-2004 (Krivovo et al., 2007), concatenated with observations from the Total Irradiance Monitor (TIM) on NASA's Solar Radiation and Climate Experiment (SORCE) from 2005-2011 (Kopp and Lean, 2011). 4.56 watts are added to the TIM measurements as previous reconstructions were calibrated against less accurate measuring equipment, compared with the TIM instrument, which led to an overestimation of TSI.

Figure A10: Updated age-depth model for Cariaco core 1002D. Original model (Haug et al., 2001) has been based on a linear interpolation of calibrated ages. We applied a 4th order polynomial fit through modelled ages calculated with a P-sequence model (Oxcal 4.2) (Bronk Ramsey, 2009, 2016): $k = 10$, Marine13 calibration curve, $\Delta R = 15 \pm 50$, one outlier: NSRL-13050.



Fig. 1

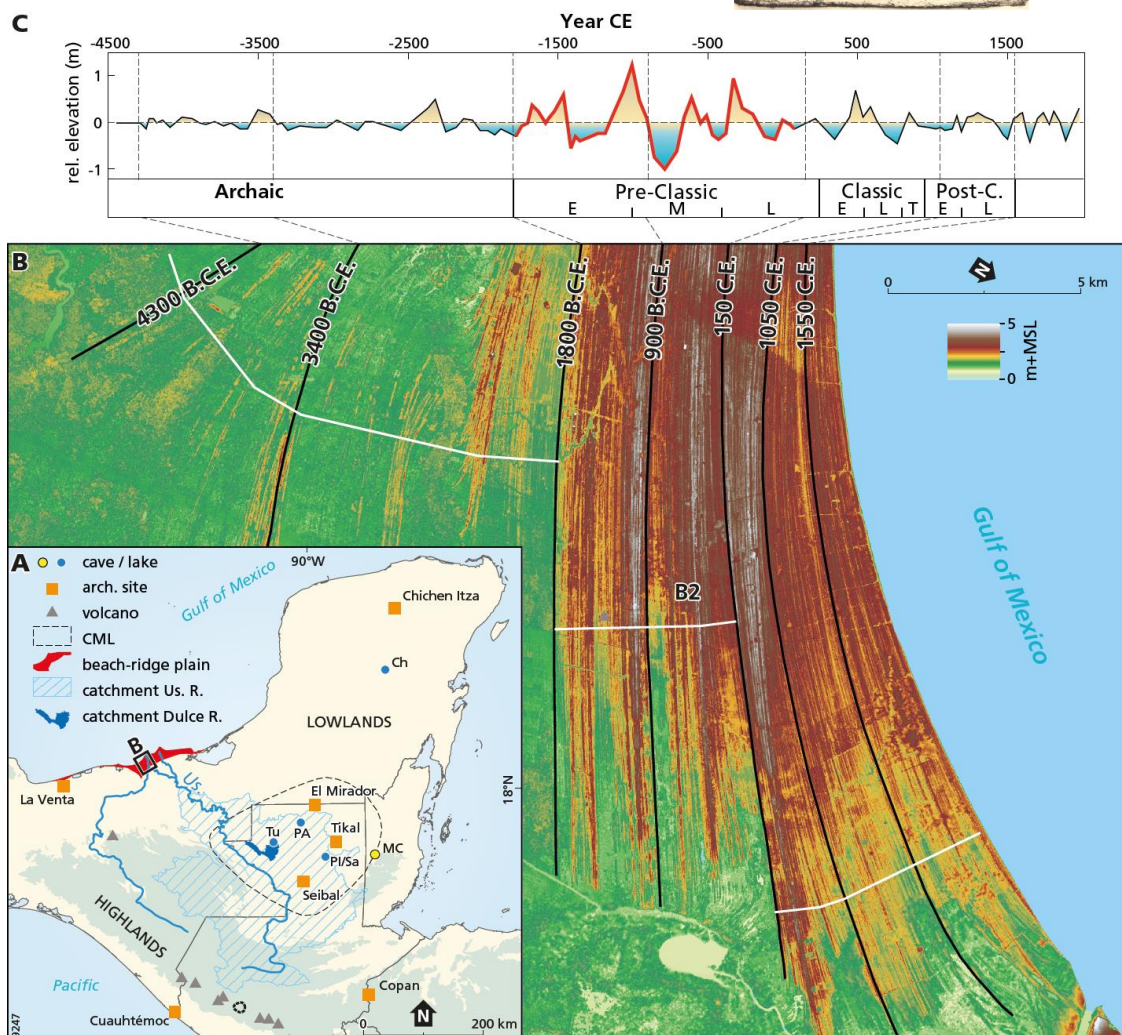


Fig. 2

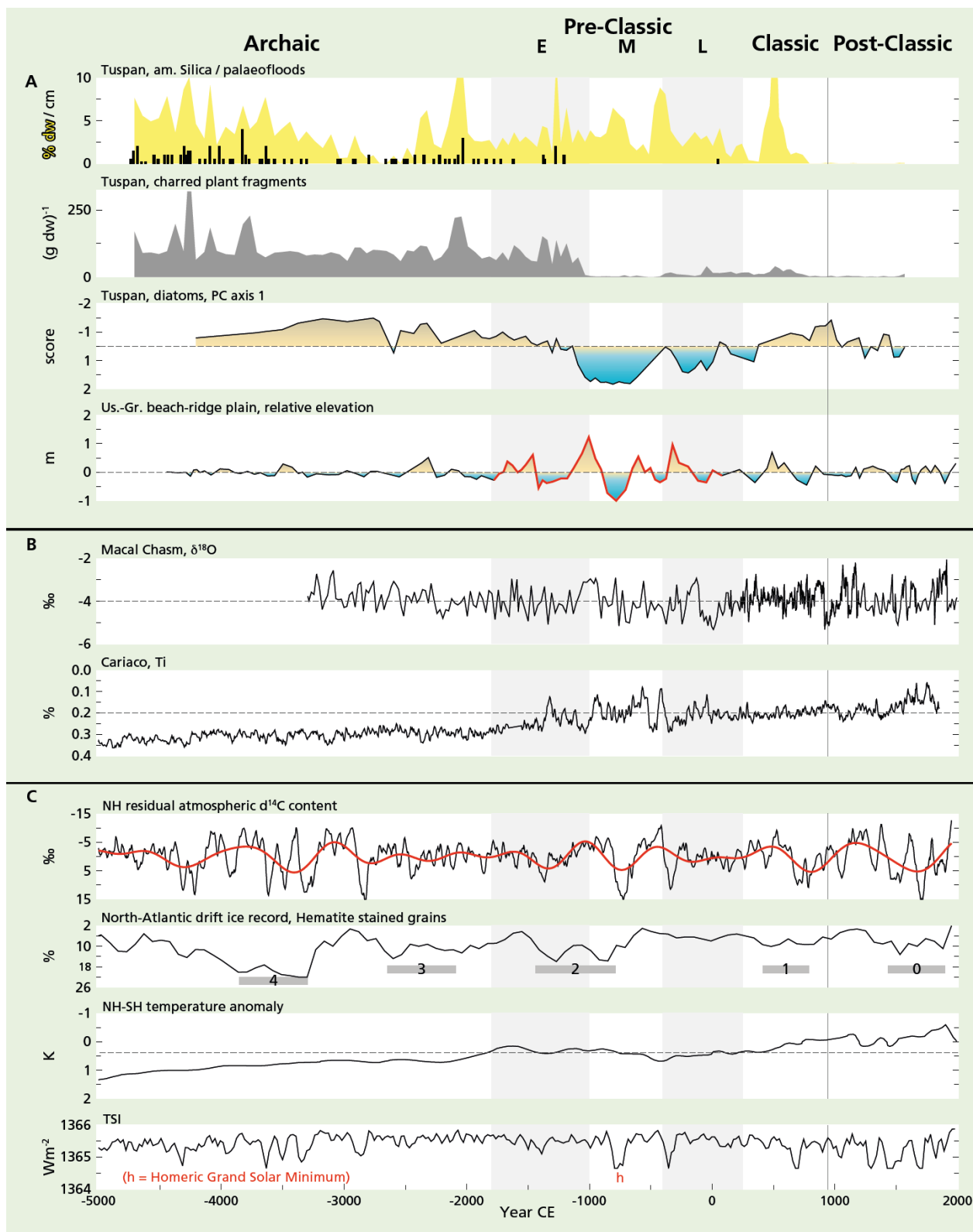


Fig. 3

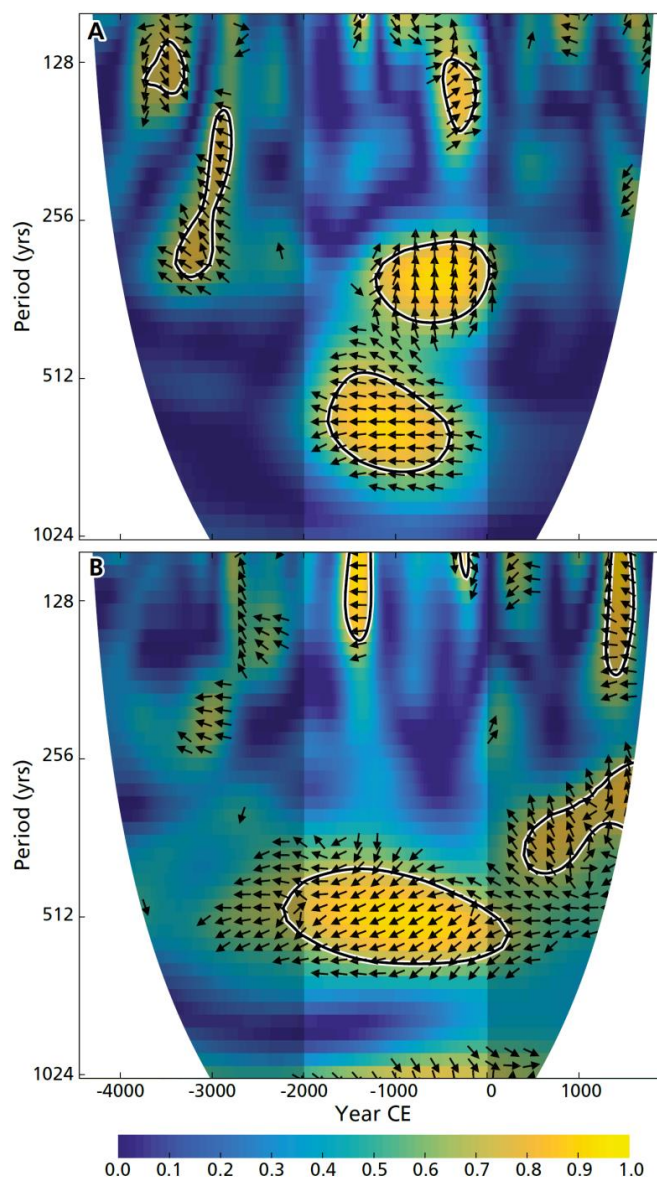
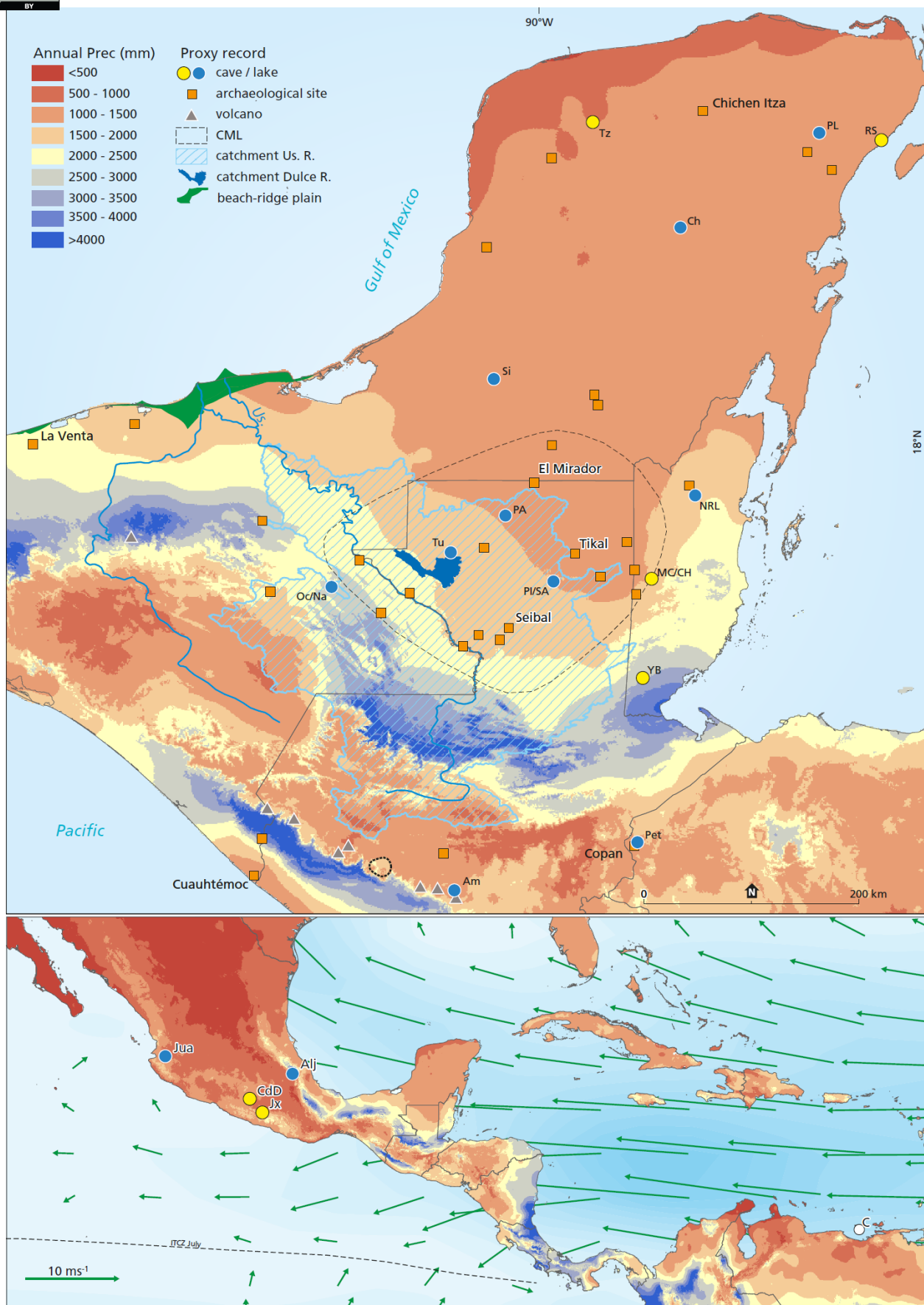


Fig. 4



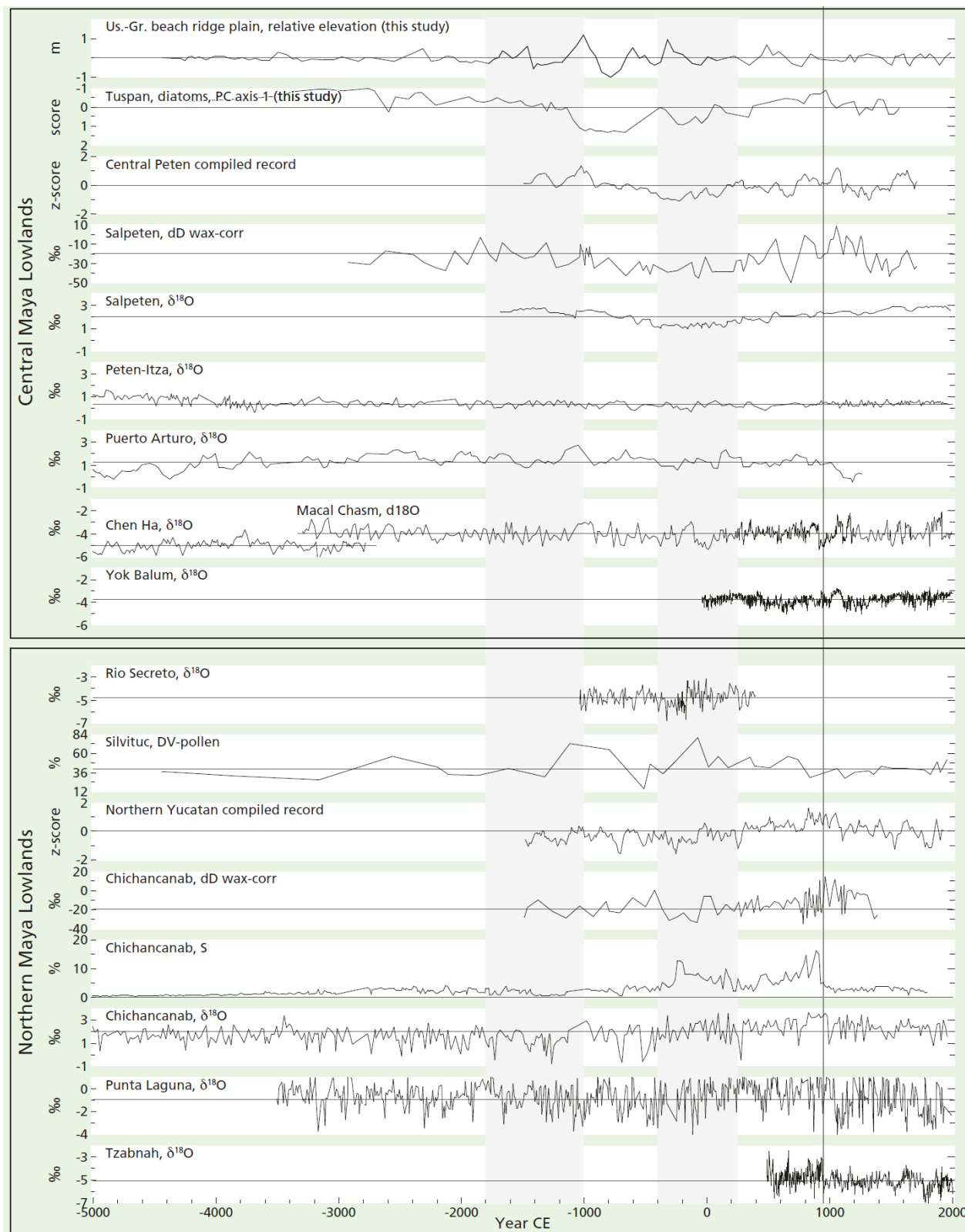


Fig. A2a

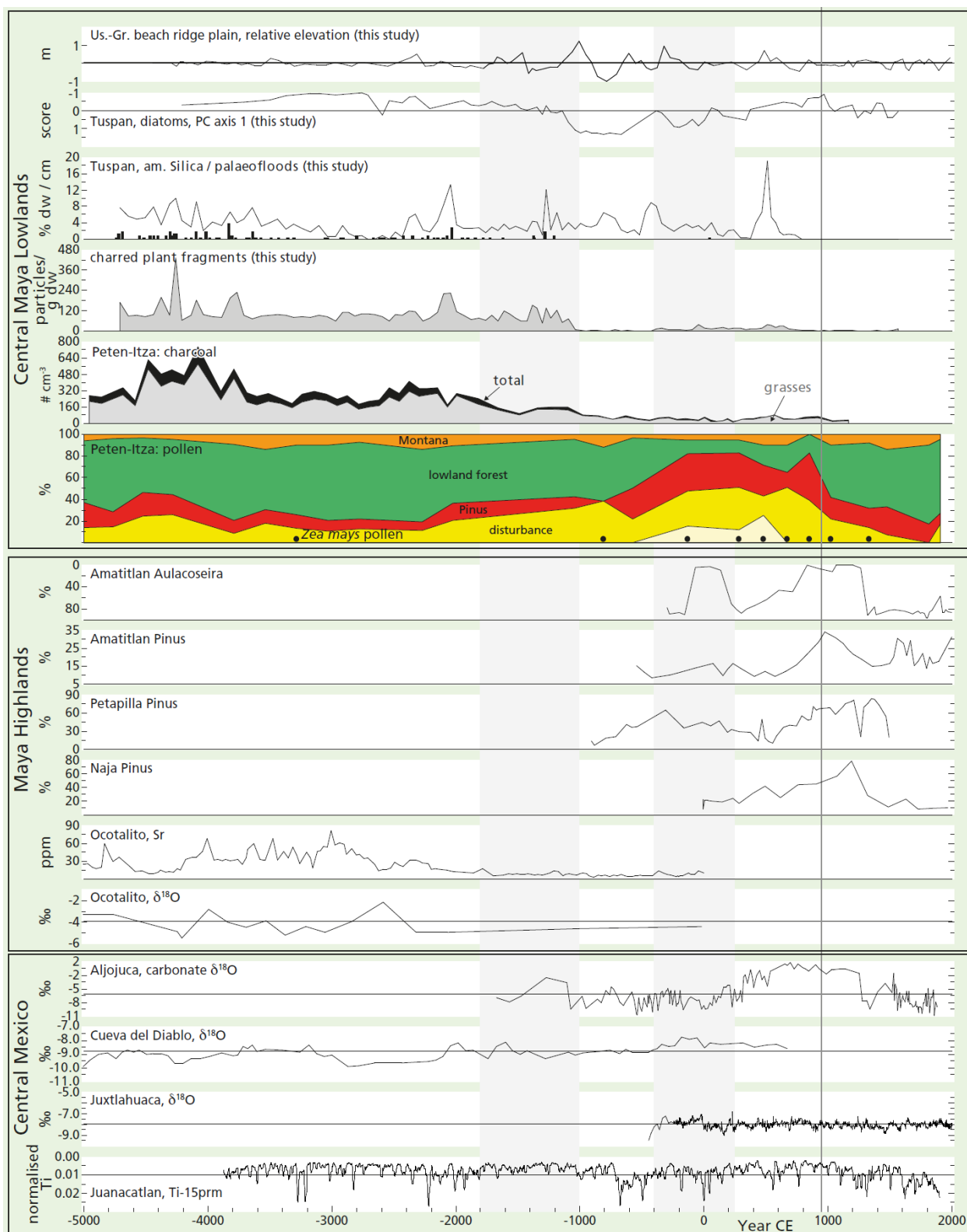


Fig. A2b

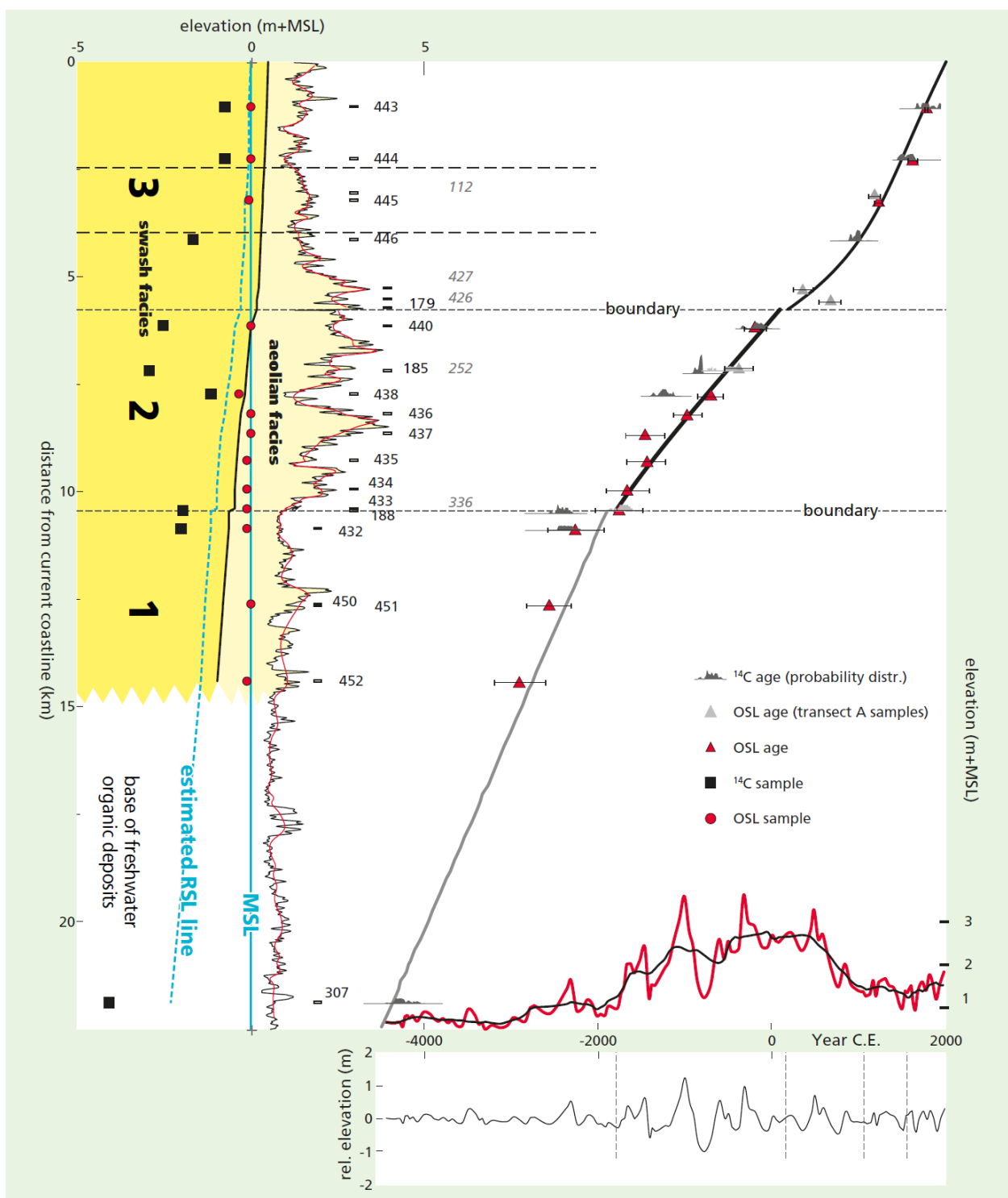


Fig. A3

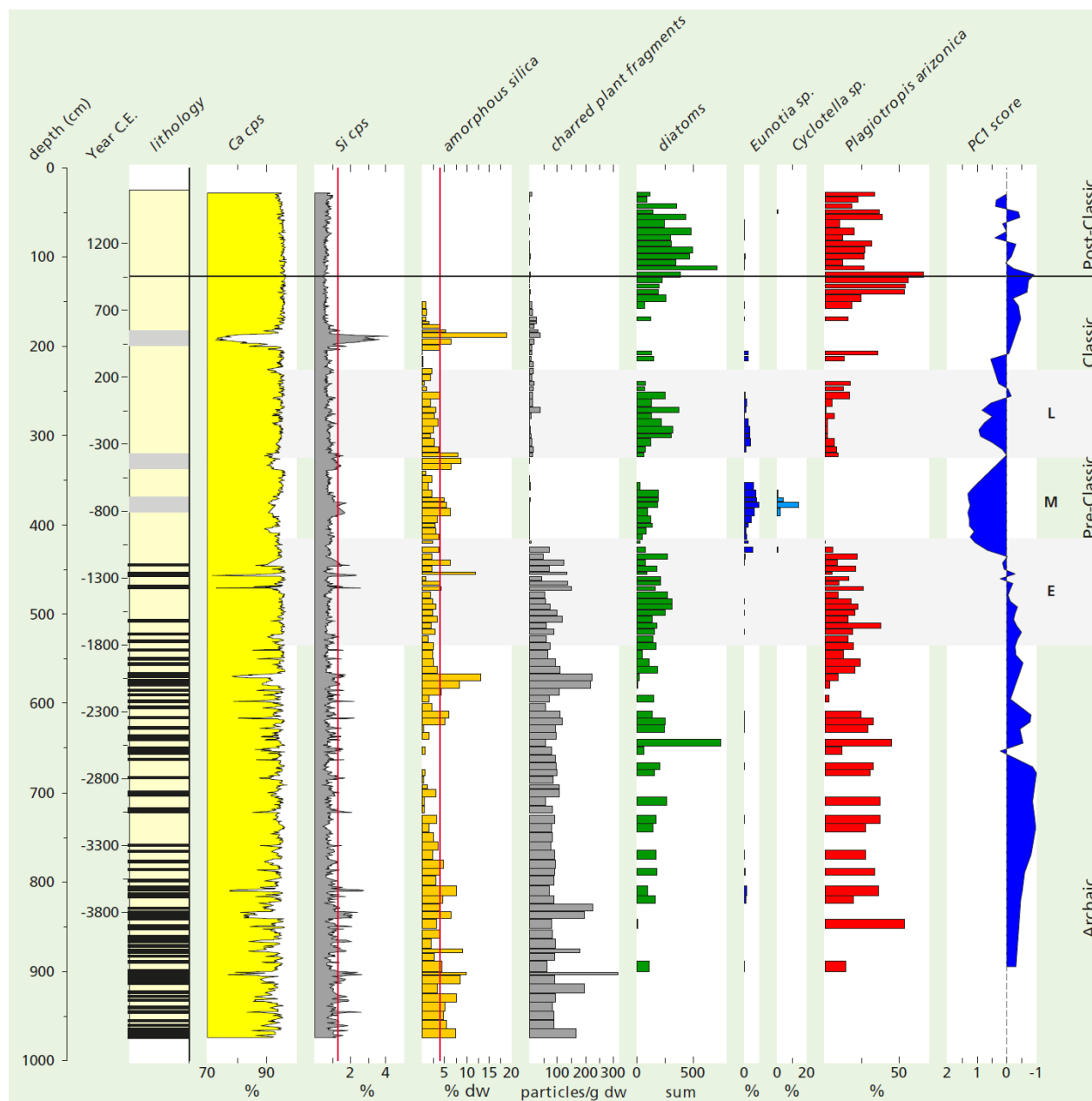


Fig. A4

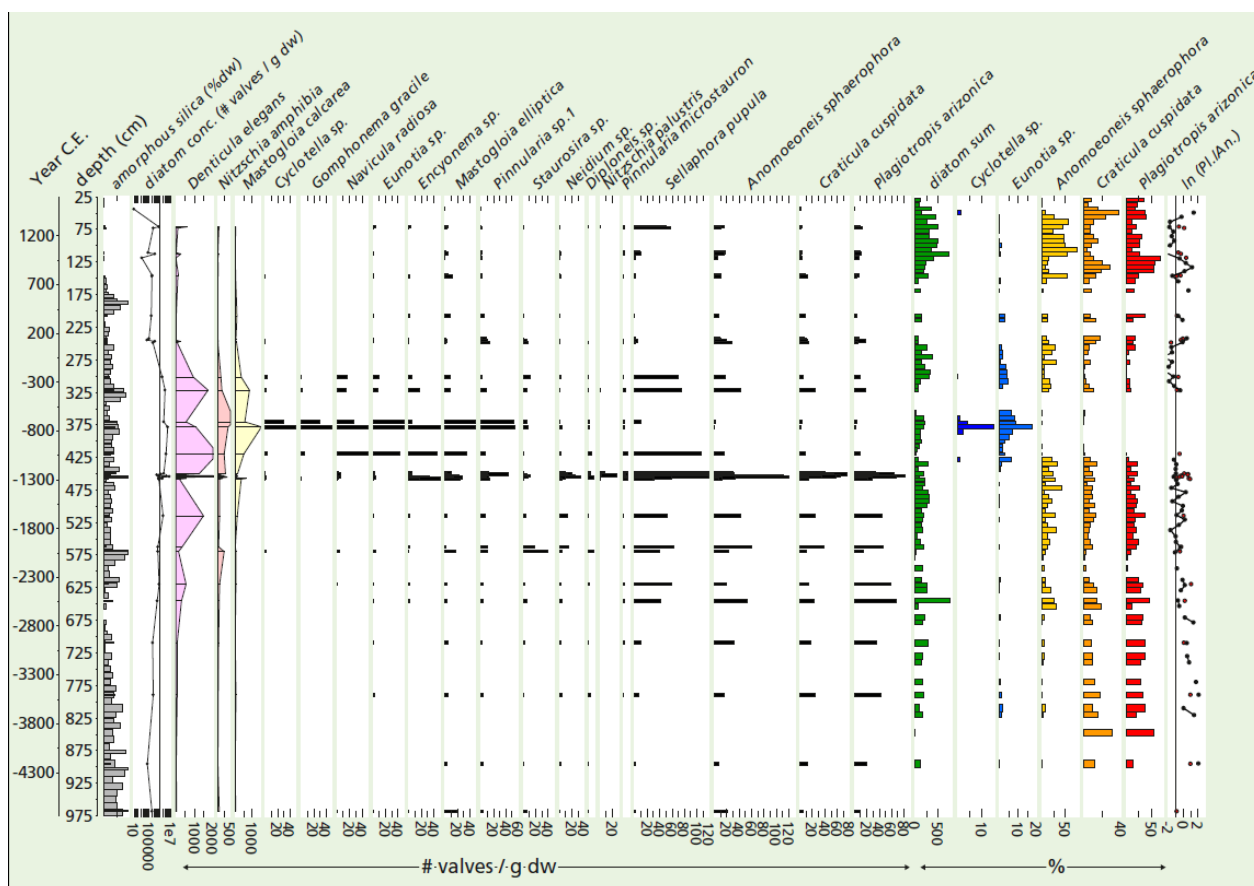


Fig. A5

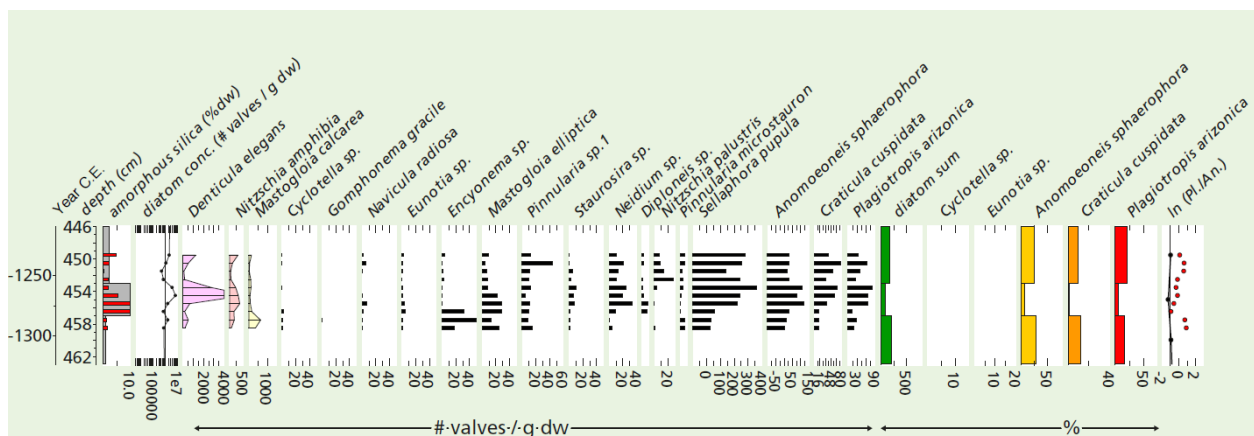


Fig. A6

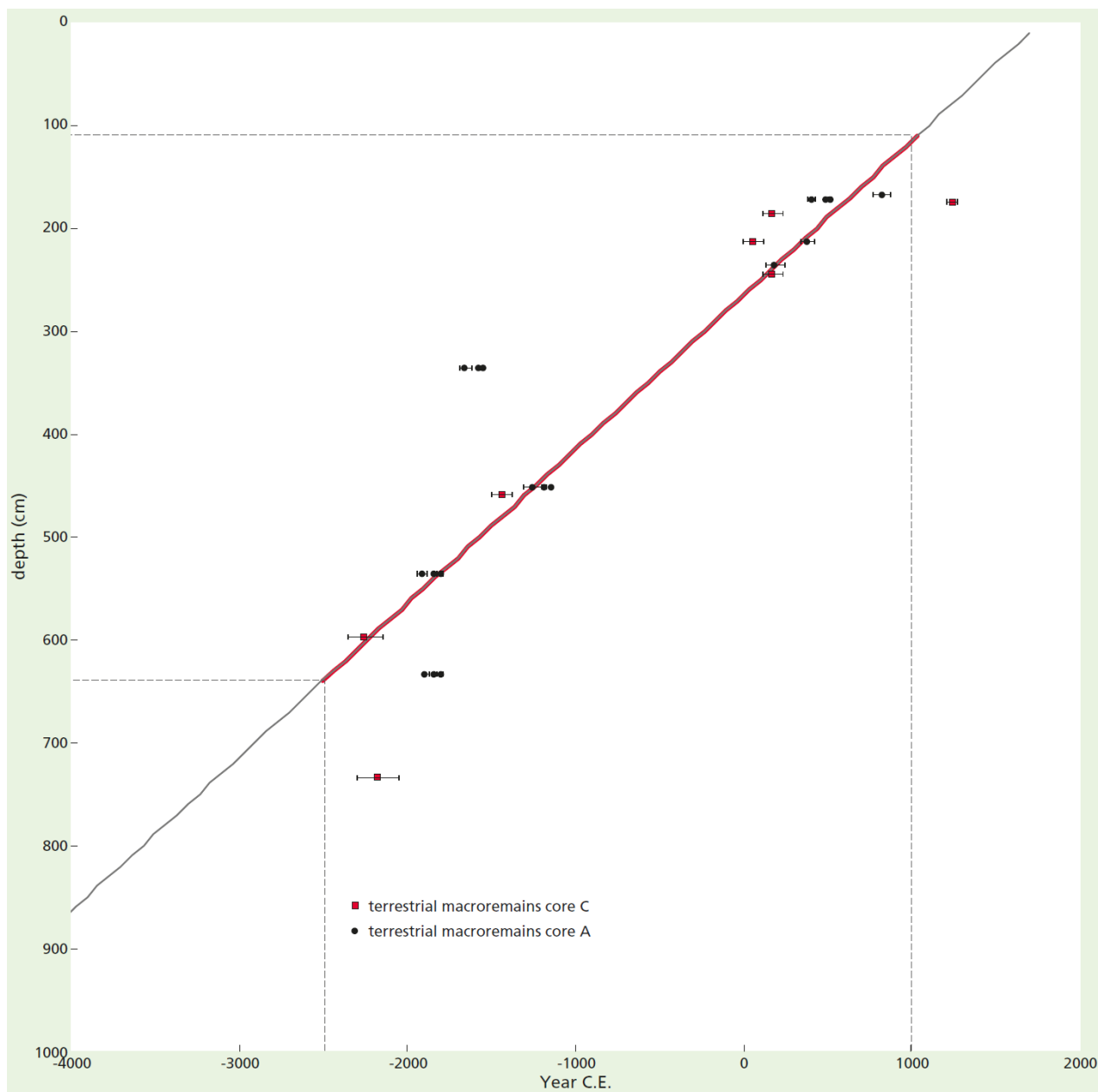


Fig. A7

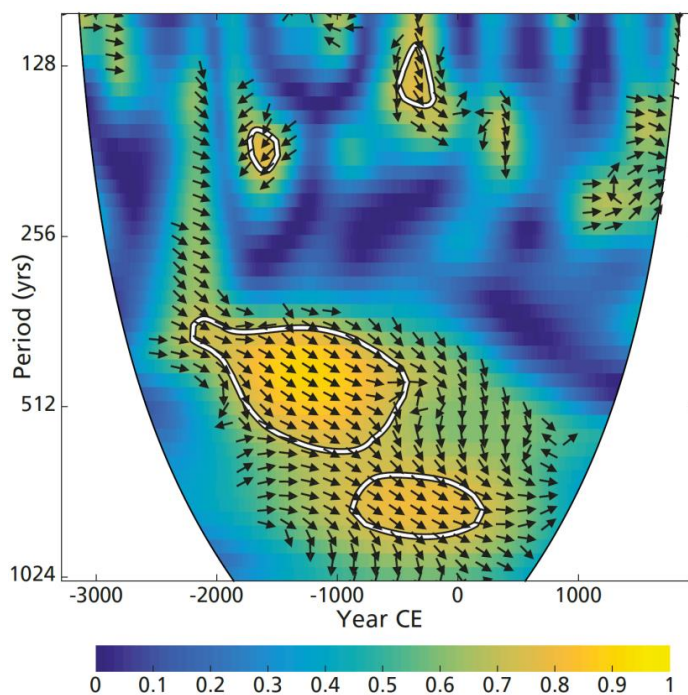


Fig. A8

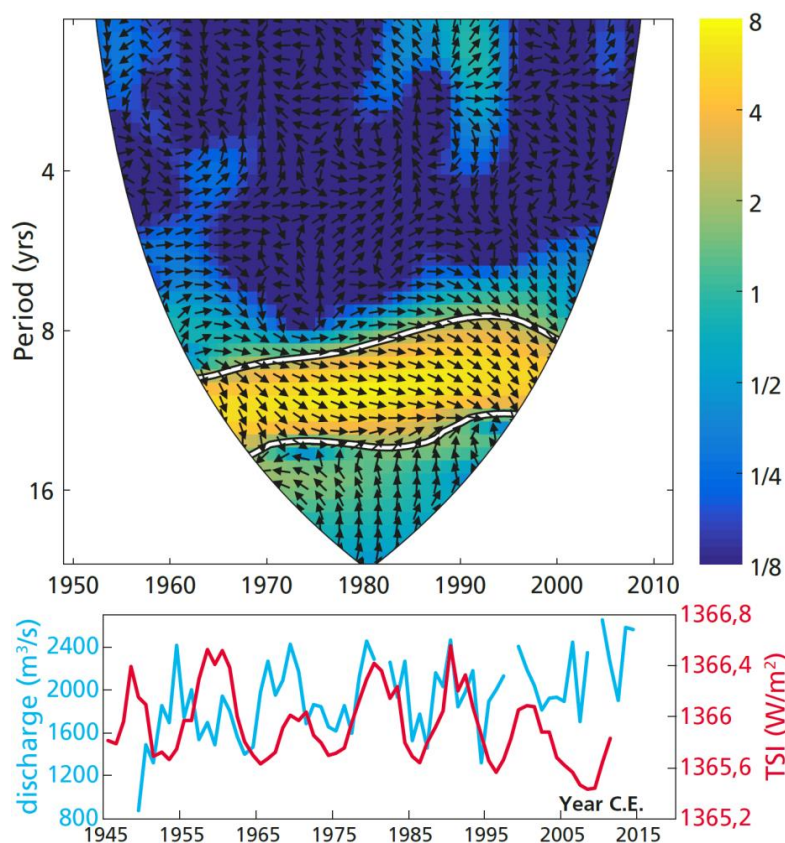


Fig. A9

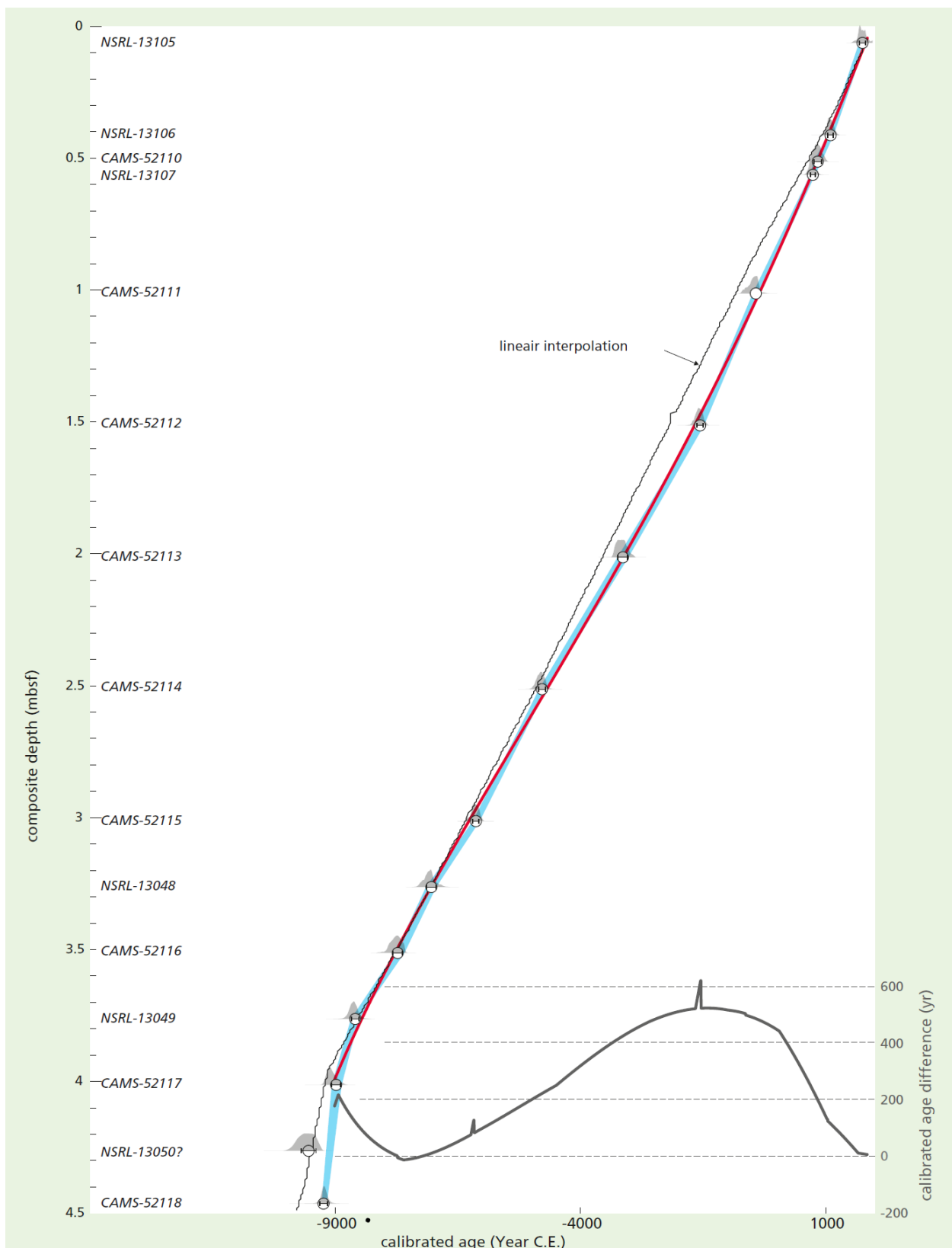


Fig. A10